Supplemental Figures

Figure S1, (Related to Figure 1 and 2) Loss-of-function in the CED pathway prevent elimination of presynaptic components. (A and B) Rab-3-mCherry is co-localized with SNB-1-GFP and SYD-2-GFP in L1 control animals. (C) The alignment of *C. elegans* CED-3 and its homolog in fly, mouse and human. The red rectangle highlights the mutation in *ju1056* animals. (D) The SNB-1-GFP puncta in D/V neurites of CED mutants have similar size and fluorescence intensity with those in synapses of DD motor neurons. A single transgene *juIs1* (Punc-25::SNB-1-GFP) was used to visualize synapses from DD neurons and RME neurons . (E) Quantification of average SNB-1-GFP intensity in the cell bodies of ctrl and mutant animals. Scale bar: 10μm. *ns*: no significant different.

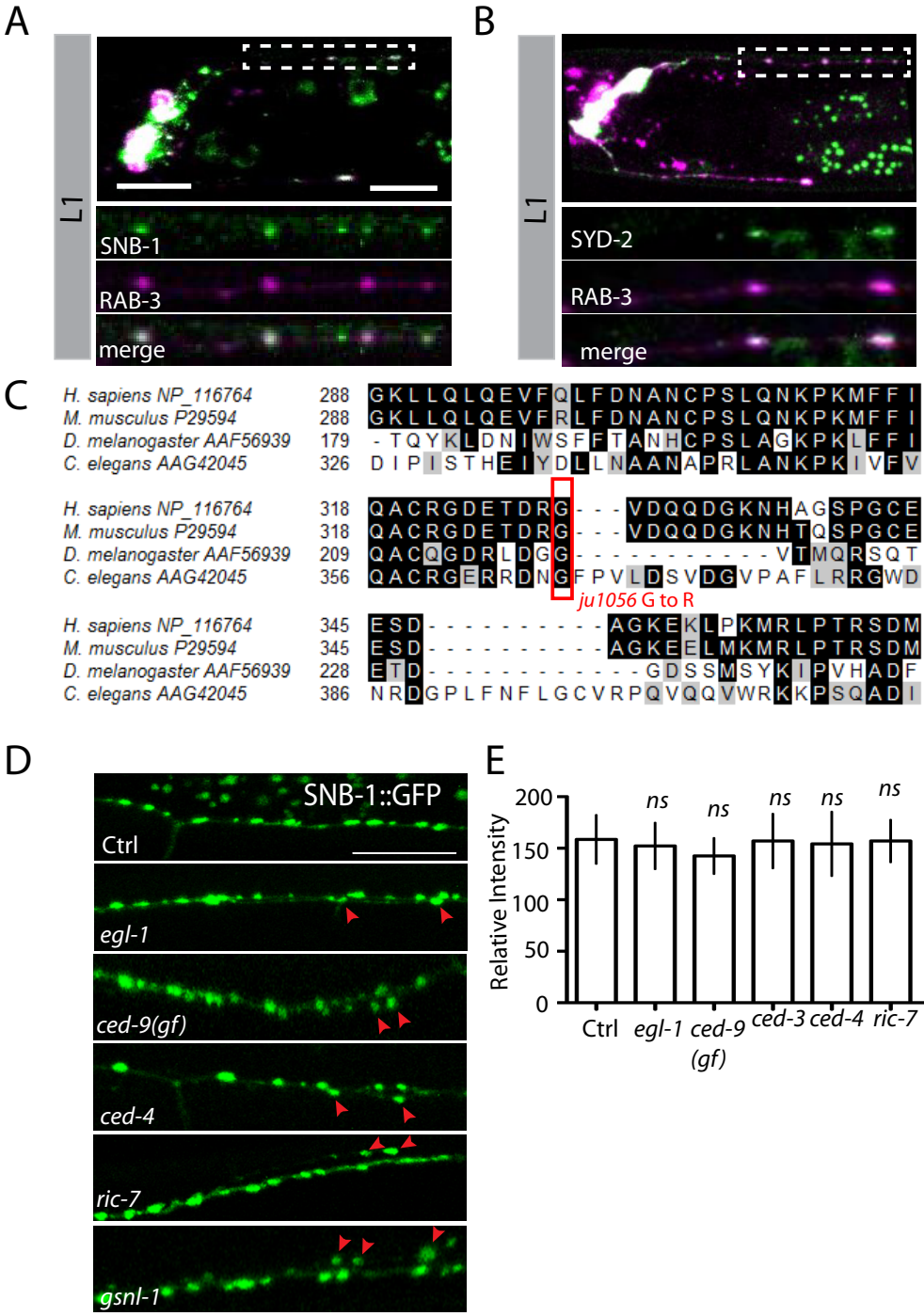
A
L1
SNB-1
RAB-3
merge
B
L1
SYD-2
RAB-3
merge
C
H. sapiens NP_116764 288 GKLLQLQEVFQLFDNANCPSLQNKPKMFFI
M. musculus P29594 288 GKLLQLQEVFRLFDNANCPSLQNKPKMFFI
D. melanogaster AAF56939 179 -TQYKLDNIWSFFTANHCPSLAGKPKLFFI
C. elegans AAG42045 326 DIPISTHEIYDLLNAANAPRLANKPKIVFV
H. sapiens NP_116764 318 QACRGDETDRG---VDQQDGKNHAGSPGCE
M. musculus P29594 318 QACRGDETDRG---VDQQDGKNHTQSPGCE
D. melanogaster AAF56939 209 QACQGDRLDGG----------VTMQRSQT
C. elegans AAG42045 356 QACRGERRDNGFPVLDSVDGVPAFLRRGWD
ju1056 G to R
H. sapiens NP_116764 345 ESD---------AGKEKLPKMRLPTRSDM
M. musculus P29594 345 ESD---------AGKEELMKMRLPTRSDM
D. melanogaster AAF56939 228 ETD----------GDSSMSYKIPVHADF
C. elegans AAG42045 386 NRDGPLFNFLGCVRPQVQQVWRKKPSQADI
D
SNB-1::GFP
Ctrl
egl-1
ced-9(gf)
ced-4
ric-7
gsnl-1
E
Relative Intensity
200
150
100
50
0
ns
ns
ns
ns
ns
ns
Ctrl
egl-1
ced-9 (gf)
ced-3
ced-4
ric-7
gsnl-1

Figure S2, (Related to Figure 1 and Figure 2) The ultrastructural morphology of the RMED/V neurites, and the synapse elimination phenotype of DD motor neurons in *ced-3(lf).* (A) A 3D reconstruction of the posterior dendritic processes of RMED (top) and RMEV (bottom) from 70nm serial sections. Both processes show periodic swellings that contain vesicular structures, but no mature presynaptic structural features (grey: neuron outline; black: nuclei; purple: mitochondria). In set are single images from indicated swellings. RME neurites are indicated by a white arrow. Mitochondria are indicated by "M". Vesicular structures of unknown identity are indicated by a black circle. Scale bars: 3μm (black) and 300nm (white). RMED/V neurites were fully reconstructed, with the exception of a 1μm-section (denoted by slashes) where we could not reliably trace the RME processes. (B) A complete set of serial sections spanning a swelling in RMED, indicated by a white arrowhead. A presynaptic specialisation from a DA or DB motor neuron is indicated by a white circle. This is a classical presynapse with an electron-dense active zone, and cluster of synaptic vesicles. The scale bar indicates 300nm. (C) Graph shows the quantification of synapse elimination defects of *ced-3(lf)* animals at L4, day one adult and day two adult stages. Experiments were performed at least 3 times, with N ≥80 animals each time. (D) Quantification data show the SNB-1-GFP puncta number in RMED/V neurites of CED, *ric-7(lf)* and *ric-7* CED double mutants. Data is shown as mean ± SD. *ns*: no significant different.

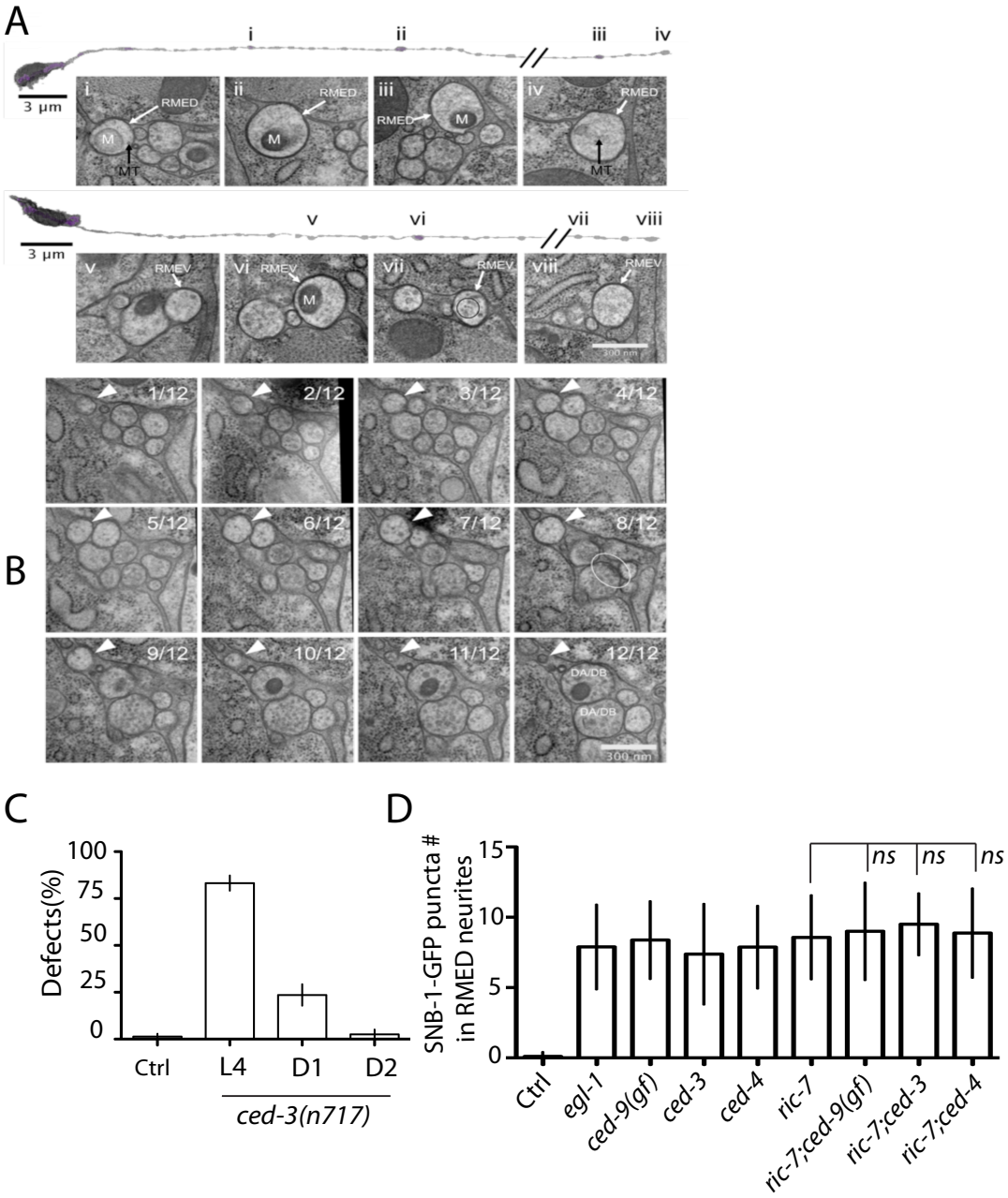
A
i
ii
iii
iv
3 µm
RMED
M
MT
v
vi
vii
viii
RMEV
B
1/12
2/12
3/12
4/12
5/12
6/12
7/12
8/12
9/12
10/12
11/12
12/12
DA/DB
C
Defects(%)
100
75
50
25
0
Ctrl
L4
D1
D2
ced-3(n717)
D
SNB-1-GFP puncta # in RMED neurites
15
10
5
0
ns
Ctrl
egl-1
ced-9(gf)
ced-3
ced-4
ric-7
ric-7;ced-9(gf)
ric-7;ced-3
ric-7;ced-4

Figure S3, (Related to Figure 3). The axonal and synaptic localization of CED-3 and CED-9 depends on mitochondria. (A) In DD motor neurons mitochondria (labeled by Cox-8-Crimson) are enriched at synaptic regions (labeled by SNB-1-GFP). Right side images are enlarged views of a single synapse. (B) CED-3 localizes at synaptic regions. The top image shows the localization of mCherry-CED-3. The middle one shows synapses (labeled by Synaptobrevin-GFP). The merged images are shown at the bottom. (C) CED-3 co-localizes with mitochondria. Mitochondria are labeled by Cox-8-Crimson. CED-3 is visualized by GFP-CED-3. (D-E) The axonal localization of CED-3 and CED-9 requires the present of mitochondria in axons. Images shows localization of mCherry-CED-3 (D) and GFP-CED-9(E) in wild type and *ric-7(lf)* animals. CB: cell bodies. (F) EGL-1 localizes to RMED/V synaptic regions in L1 control animals. (G) *unc-116* is not required for D/V neurite localization of mitochondria. Images (H) and quantification (I) show that overexpression of mitochondrion targeted kinesin did not rescue SNB-1-GFP distribution defects in *ric-7(lf)* animals. Scale bar, 10 μm. *ns*: no significant different.

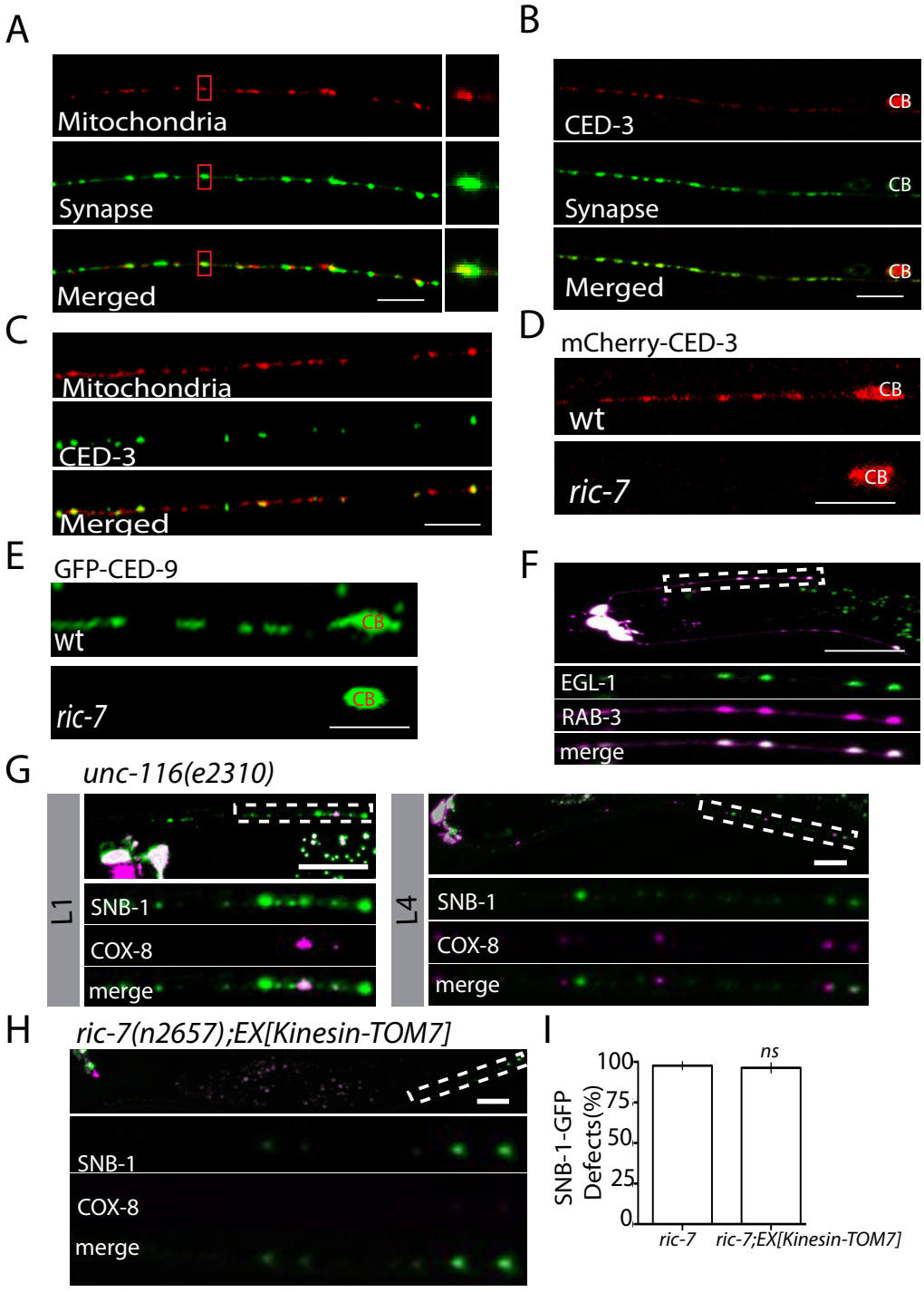
A
Mitochondria
Synapse
Merged
B
CED-3
Synapse
Merged
CB
C
Mitochondria
CED-3
Merged
D
mCherry-CED-3
wt
ric-7
E
GFP-CED-9
wt
ric-7
F
EGL-1
RAB-3
merge
G
unc-116(e2310)
L1
L4
SNB-1
COX-8
merge
H
ric-7(n2657);EX[Kinesin-TOM7]
I
SNB-1-GFP Defects(%)
100
75
50
25
0
ns
ric-7
ric-7;EX[Kinesin-TOM7]

Figure S4, (Related to Figure 3). The axonal and synaptic localization of mitochondria is independent on the CED pathway. (A-E) Confocal images show that loss-of-function in the CED pathway does not altered the localization of mitochondria in D/V neurites in L1 or adult animals. Scale bar, 10 μm.

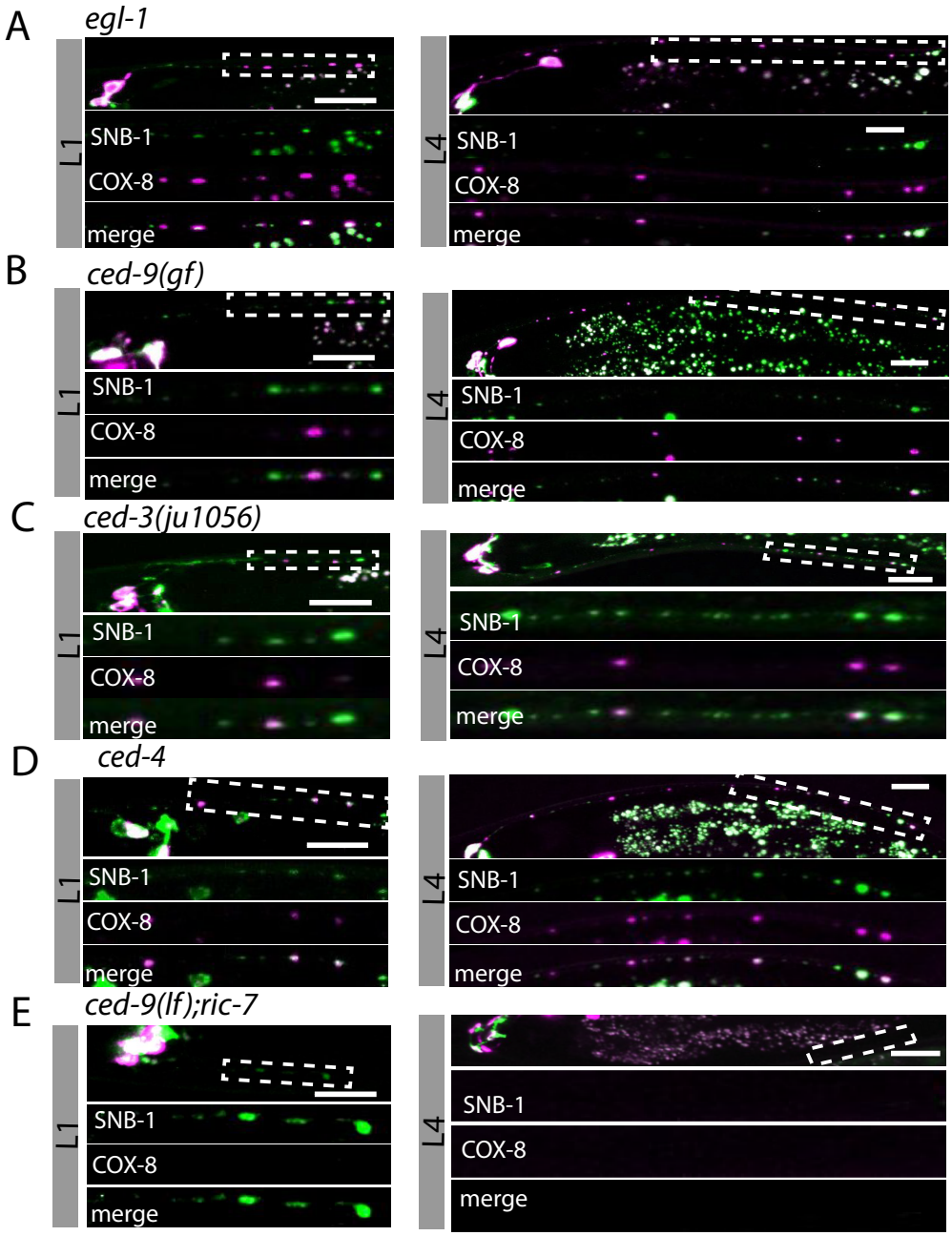
A
egl-1
L1
SNB-1
COX-8
merge
L4
SNB-1
COX-8
merge
B
ced-9(gf)
L1
SNB-1
COX-8
merge
L4
SNB-1
COX-8
merge
C
ced-3(ju1056)
L1
SNB-1
COX-8
merge
L4
SNB-1
COX-8
merge
D
ced-4
L1
SNB-1
COX-8
merge
L4
SNB-1
COX-8
merge
E
ced-9(lf);ric-7
L1
SNB-1
COX-8
merge
L4
SNB-1
COX-8
merge

Figure S5, (Related to Figure 3 and Figure 4). Loss-of-function in *ric-7* suppresses synapse elimination in DD motor neurons, and *gsnl-1* mutation. Images (A) and Quantification (B) of synapse elimination defects in *ric-7(lf)* animals at L4 stage. Experiments were performed at least 3 times, with N ≥80 animals each time. Data is shown as mean ± SD. Student test, ** P < .01. Scale bar, 10 μm. (C) The alignment of *C. elegans gsnl-1* and its homolog in fly, mouse and human. The red rectangle highlights the mutation in *ju1061* animals and the CED-3 cleavage sites.

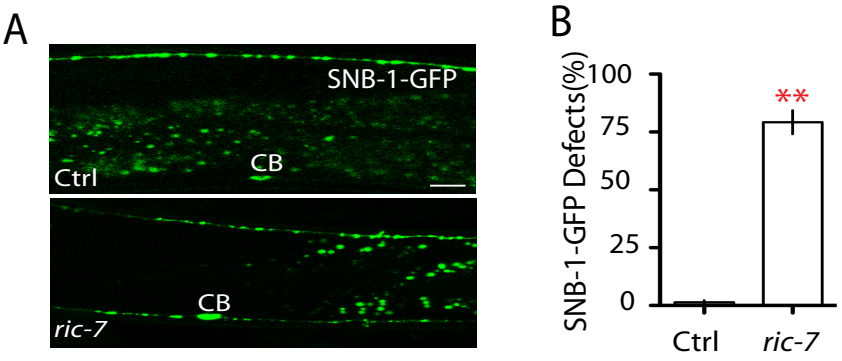
A
SNB-1-GFP
Ctrl
CB
CB
ric-7
B
SNB-1-GFP Defects(%)
100
75
50
25
0
**
Ctrl
ric-7
C
M. musculus O88398
H. sapiens O75366
Danio rerio NP_835232
C. elegans CAA94782
ju1061 W to stop codon
Gelsolin domain 3
CED-3 cleavage site
Gelsolin domain 4

Figure S6 (Related to Figure 4). Loss-of-function in *gsnl-1* suppresses elimination of presynaptic components in RME neurons. Images(A) and Quantification (B) of active zone elimination defects in *gsnl-1(ok2979)* animals. (C) Loss-of-function in *gsnl-1(ok2979)* does not change mitochondrion localization. (D) F-actin is accumulated in both axons and dendrites in DD neurons. Rab-3-mCherry (Pink color) is used to label presynaptic vesicles in axons. GFP-UtrCH is used to label F-actin (Green color). Images (F) and quantification data show that loss-of-function in *gsnl-1* induced mis-accumulation of F-actin at transient synapses. Red arrowheads highlight the enlarged mis-accumulated F-actin patches at un-eliminated transient synapses. N> 20 animals. (G) Double mutants of *gsnl-1(ok2979)* and *ced-3 (ju1056)* do not change the average SNB-1-GFP puncta number in D/V neurites. Experiments were performed at least 3 times, with N ≥80 animals each time. Data is shown as mean ± SD. Student test, ** P < .01. Scale bar, 10 μm.

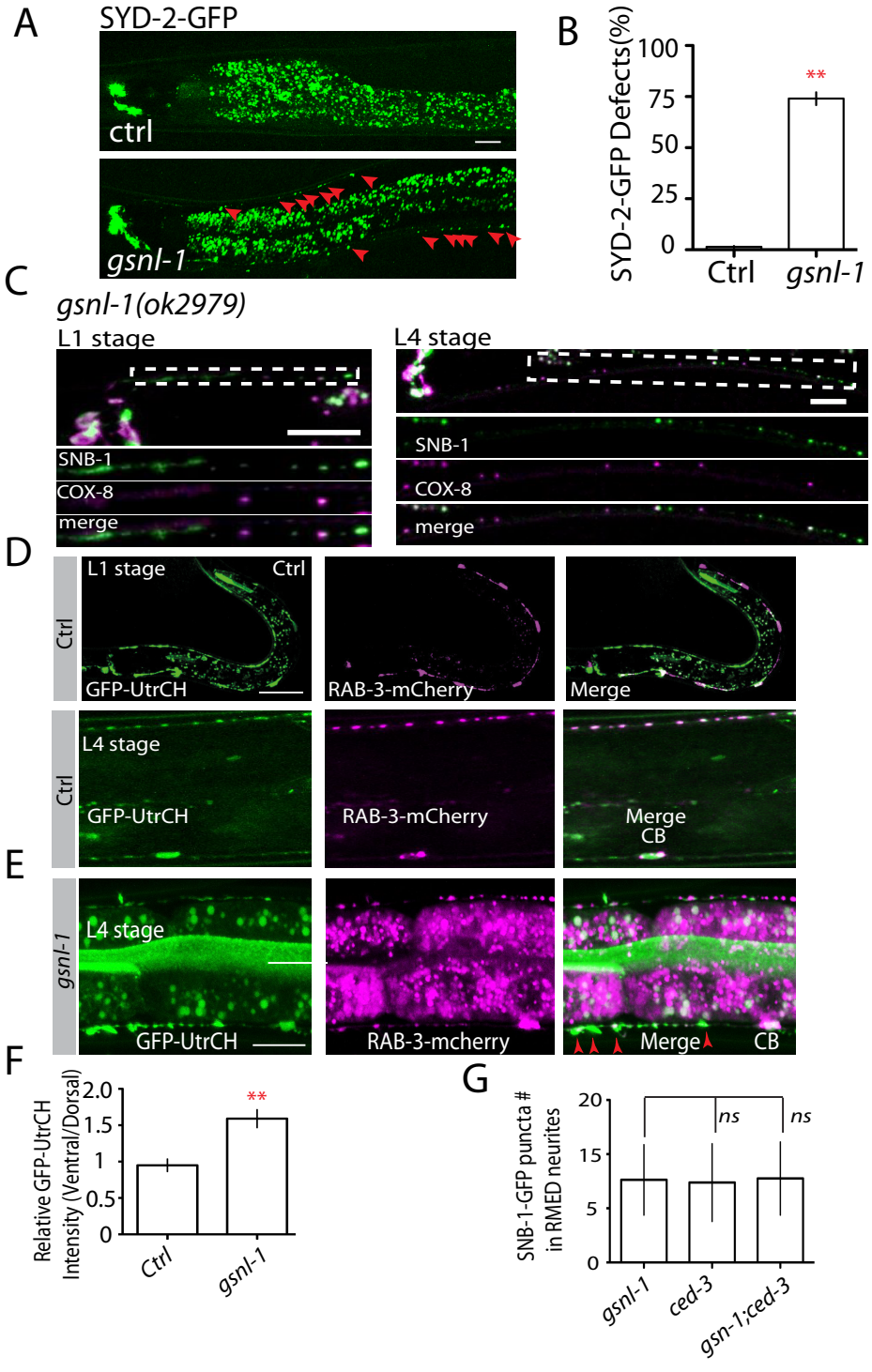
A
SYD-2-GFP
ctrl
gsnl-1
B
SYD-2-GFP Defects(%)
100
75
50
25
0
**
Ctrl
gsnl-1
C
gsnl-1(ok2979)
L1 stage
L4 stage
SNB-1
COX-8
merge
D
L1 stage
Ctrl
GFP-UtrCH
RAB-3-mCherry
Merge
L4 stage
Merge CB
E
gsnl-1
RAB-3-mcherry
CB
F
Relative GFP-UtrCH Intensity (Ventral/Dorsal)
2.0
1.5
1
0.5
0
G
SNB-1-GFP puncta # in RMED neurites
20
15
5
0
ns
ced-3
gsn-1;ced-3

Figure S7 (Related to Figure 4 and Figure 6). Loss-of-function in *gsnl-1* suppresses synapse elimination in DD motor neurons, and mitochondria and the CED pathway regulate F-actin disassembly through GSNL-1.

Images (A) and Quantification (B) of synapse elimination defects in *gsnl-1(ok2979)* animals. Experiments were performed at least 3 times, with N ≥80 animals each time. Loss-of-function in *egl-1*(C), *ric-7*(E) and gain-of-function in *ced-9*(D) promotes F-actin assembly in D/V neurites, and overexpression of P40 suppressed these phenotypes. Images (F) and quantification data (G) show loss-of-function in the CED pathway and *ric-7* induces mis-accumulation of F-actin at dorsal cords of DD neurons in L4 animals. Red arrowheads highlight the enlarged mis-accumulated F-actin patches at un-eliminated transient synapses. N> 20 animals. Data is shown as mean ± SD. Student test, ** P < .01. Scale bar, 10 μm.

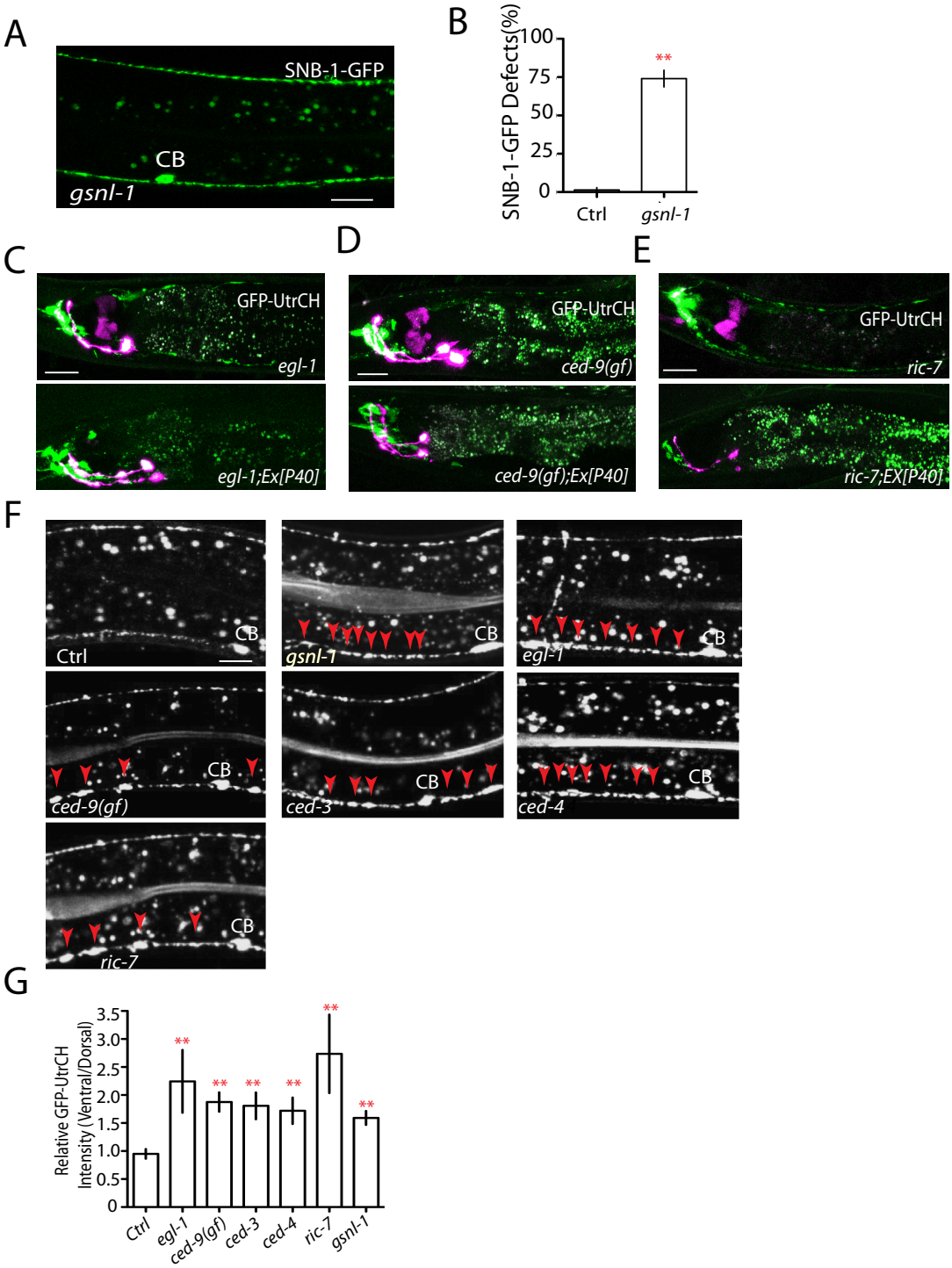
A
SNB-1-GFP
CB
gsnl-1
B
SNB-1-GFP Defects(%)
100
75
50
25
0
**
Ctrl
gsnl-1
C
GFP-UtrCH
egl-1
egl-1;Ex[P40]
D
GFP-UtrCH
ced-9(gf)
ced-9(gf);Ex[P40]
E
GFP-UtrCH
ric-7
ric-7;EX[P40]
F
Ctrl
gsnl-1
egl-1
ced-9(gf)
ced-3
ced-4
ric-7
CB
G
Relative GFP-UtrCH Intensity (Ventral/Dorsal)
3.5
3.0
2.5
2.0
1.5
1.0
0.5
0
**
Ctrl
egl-1
ced-9(gf)
ced-3
ced-4
ric-7
gsnl-1

References:

Hatzold, J., and Conradt, B. (2008). Control of apoptosis by asymmetric cell division. PLoS biology 6, e84.

Hengartner, M.O., and Horvitz, H.R. (1994). Activation of C. elegans cell death protein CED-9 by an amino-acid substitution in a domain conserved in Bcl-2. Nature 369, 318-320.

Rawson, R.L., Yam, L., Weimer, R.M., Bend, E.G., Hartwieg, E., Horvitz, H.R., Clark, S.G., and Jorgensen, E.M. (2014). Axons degenerate in the absence of mitochondria in C. elegans. Current biology : CB 24, 760-765.

Yuan, J., and Horvitz, H.R. (1992). The Caenorhabditis elegans cell death gene ced-4 encodes a novel protein and is expressed during the period of extensive programmed cell death. Development 116, 309-320.